Digital image correlation, acoustic emission and in-situ microscopy in order to understand composite compression damage behavior

Khalil Hamdi, Gurvan Moreau, Zoheir Aboura

Digital Image correlation, acoustic emission and in-situ microscopy in order to understand composite compression damage behavior.

Khalil HAMDI [a,*], Gurvan MOREAU [b], Zoheir ABOURA [a]

[a)1] *Université de technologie de Compiègne, CNRS, Roberval (Mechanics, energy and electricity), Centre de recherche Royallieu - CS 60 319 - 60 203 Compiègne Cedex*

[b)] *Safran Composites, a technology platform of Safran Tech, 33 avenue de la Gare, 91760 ITTEVILLE, France*

[*)] *Corresponding author: khalil.hamdi@utc.fr; khalilhamdi@hotmail.fr*

Digital Image correlation, acoustic emission and in-situ microscopy in order to understand composite compression damage behavior.

Abstract

In this work, a description of carbon fiber reinforced polymers (CFRP) compression-damaging scenario from first micro-damages to final failure of the material and potential effect of matrix (resin) on compressive mechanical properties and the damaging scenario is given. For that, two types of CFRP with the same woven reinforcement but with different resin were tested. First, combined load compression (CLC) tests were performed and the macroscopic compression behavior was then compared between the different materials. Then, analysis of the CLC testing with the multi-instrumentation was conducted to describe all the damage steps progression. Digital image correlation (DIC), acoustic emission (AE) and in-situ microscopy were the three parts of the multi-instrumentation. By combining the data from each technique, it was possible to verify the minor effect of the resin on the global compression behavior of composites. Signal processing tools (K-means and KNN) were used to cluster the acoustic emission signals. Three main classes were obtained and were labeled according to the possible damage scenario. This allowed the identification of the beginning of a severe damage (indicated by a noticeable rise in the measured acoustic energy) which was different depending on the matrix.

Keywords: Carbon Fiber Reinforced Polymers (CFRTP), Compression behavior, resin effect, digital image correlation,acoustic emission, k-means, KNN, signal processing.

Introduction

Carbon fiber reinforced polymers laminates show very interesting mechanical properties especially for tensile stress (modulus and strength). Nevertheless, one of their weaknesses in axial loading is their compressive behavior. Indeed, the axial compression may induce bending due to local fiber curvature (Figure 1). In the case of woven reinforced composites, the fibers are also affected by the deformation of the neighboring tows. It is also obvious that friction between fibers and fiber/matrix take place. In a global approach, basic information about compressive failure mechanisms on UD reinforcement mention kinking [1, 2] and tows splitting [3] as major causes of composites failure. Nevertheless, as detailed, chronological damage progressions (damage scenario) might be more complex in woven composites where two or more mechanisms take place simultaneously.

Figure 1 : Curvature increasing of longitudinal fibers under compressive load

Several studies have been dedicated to compression damage in composite materials. In the literature, mainly, four failure modes are described. The most common observations are shear failure [4–6], interlaminar failure[1, 7], interfacial failure [8] and kinking failure [9, 10].The first type of damage, appears in-plane [4] or through the thickness shear [6] or through wedge splitting[5]. For the second and third type of damages mentioned observations show delamination or longitudinal cracking [1] and brooming[7, 8]. For the last failure mode, kink bands could appear in-plane[9] or out-of-plane [10].

For instance, Carvalho et al. showed that the compression failure modes might be related to crack propagation, kink Band and matrix cracking in the case of Carbon Fiber Reinforced Polymers (CFRP) [11]. Though, failure mode seems to be conditioned by the stacking sequence, a difference between materials with ordered and random stacking reinforcement was recorded. Besides modes cited previously for random stacked reinforcement composites, the ordered stacked ones showed delamination and fiber bending. Another study focused on the reinforcement architecture effect on the compression properties of composites[12]. It was shown that the compression properties are improved by minimizing fibers waviness. Plain

weave composites showed the poorest compression properties. This result was confirmed in another paper, using a computed tomography (CT) scan[13].

Taking into account all these studies, waviness is obviously detrimental to compression properties [12]. In most cases, post mortem observations were used to indicate it. Even if it is not always accurate, it might indicate the transformation of the compression effort to microbuckling of fibers leading to warp and weft separation (decohesion/delamination). As the curvature of fiber increase under compression, , shearing stress induces fibers rupture. Vieille et al. studied this topic by determining the critical stress required for buckling in compression after impact[14]. They employed deflection measurement (LVDT) and longitudinal strain (in-plane Digital Image Correlation (DIC)). According to them, microbuckling is caused by misalignment of fibers (crimp angle).With the same approach, Davidson et al. studied the effect of an induced defect on the composite compression properties. By the use of DIC, it was shown that the curvature induced by the defect leads to the major damage of the composite (strain/stress concentration). Failure in this case occurred by delamination and in plane kink band [15].

To sum up, lateral stability of fibers is a crucial parameter to maintain good compression properties of the composite material. That's why, the resin plays an important role in the compression behavior of composites. Vieille et al. have shown that the resin stiffness does not affect compression strength but it impacts the damage mechanisms. In fact, carbon fibers reinforced thermoplastics resins show clear plastic kink band starting at crimp angles in the compression after impact (CAI), in contrast, stiffer resin such as epoxy lead to failure by delamination and interlaminar cracking[14]. Authors shows clearly the effect of the matrix stiffnes on the compression damage mechanism. Few similar results exist in the literature that shed the light on the resin stiffness effect (generally, comparing thermoplastic: TP with thermoset: TS resins) on the CAI properties of composite materials[16]. Nevertheless, we notice a lack of studies focusing on compression properties of composite as a function of the used resin.

After this brief review of the literature, we propose to study the compression behavior of CFRP.

This study attempts to accurately describe CFRP compression damaging scenario from first micro-damages to final failure of the material and potential effect of matrix (resin) on compressive mechanical properties and the damaging scenario.

Two different materials with the same reinforcement but different epoxy resin types are considered. This will highlight the resin effect on the composite materials compression properties. Obviously, this is associated to the fiber lateral stability, which drastically influence compression behavior of composites. This lead us to the second part of this study regarding the damage scenarios of the composite. For this, multi-instrumentation tools are deployed to understand different phenomenon. Multi-instrumentation set-up included digital image correlation, acoustic emission and in-situ microscopy. A special effort on the acoustic emission signal processing was performed using unsupervised and supervised classification algorithms to isolate the different damage.

Experimental set-up and methods

Materials

Composite materials were provided by Safran Composites. It consisted of two types of samples depending on the matrix used for fabrication (Table 1). Both resins come frome the epoxy familybut hold different mechanical properties. R8 resin shows better mechanical performance in traction. However, correlation between resin properties and composite behavior is not established for compression. All composite material samples have the same reinforcement: carbon fabric, twill2x2 having an areal weight of 335 g/m². Laminate sequence is also the same for all materials: 10 plies [0/45/0/0/45/45/0/0/45/0]. Samples were cut to 140mm by 12mm by 3mm, and machined edges with a surface finish and roughness according to ASTM D6641allowing compression load transfer from the compression platen without crushing in the contact area (CLC testing according to ASTM D-6641[17]).The Representative Elementary Volume (RVE) of the composite materials are around 8mm by 8mm by 0.3mm wich is obviously covered by one sample.

Resin	Notations used in this study	Young's Modulus (Gpa)	Tensile strength (Mpa)
Resin 7	R7	3.33 (±4.5%)	88.04 (±2.8%)
Resin 8	R8	4.59 (±5.7%)	105.53 (±0.8%)

Table 1 : Identification of the materials used in this study and the resin mechanical properties

Methods

Compression was performed using an INSTRON 1186 mechanical testing machine equipped with a 200KN load cell. The crosshead speed was 1mm/min in the load phases. Testing was conducted refering to the ASTM D-6641 standard and,testing fixtures were as recommended in this standard and represented in Figure 2.

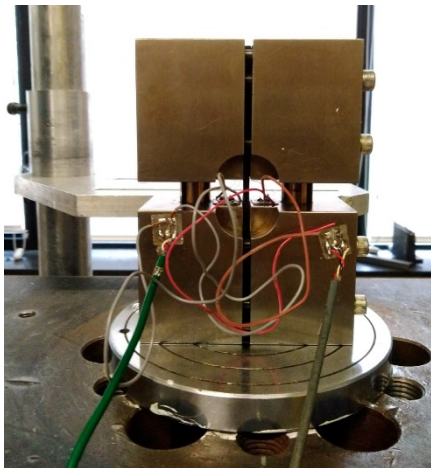

Figure 2 : Compression fixture (CLC testing)

- **Preleminary tests**

Monotonous compression tests aiming to measure compression modulus and strength were performed. Replicates were performed at least 5 times for each material. For this purpose, samples were instrumented with two back-to-back 5mm length strain gauges (manufactured by KYOWA) in order to measure longitudinal strain on each face of the sample. The nominal strain was taken as the mean value between the two signals of gauges.The size of the strain gauge was imposed by the size of the useful area. It's obvious that such a size doesn't cover up the representative volume element (RVE = 8mm by 8mm by 0.3mm) size of the material but the use of two strain gauge must confirm relevance of the measurement.

- **Multiinstrumented tests**

To collect the needed inputs, the experimental setup was upgraded by three tools of investigation: Digital Image Correlation (DIC), Acoustic Emission (AE) and in-situ microscopy.

In Figure 3, the different components of the instrumentation are represented with their respective location in regards to the specimen (the front side for acoustic emission and the edge sides for the digital image correlation and the *in-situ* microscopy). As mentioned below, testing was interrupted to allow microscopy observations: it means that the displacement was

kept constant at a certain level of the loading cycle , this leads to negligible stress relaxation (Figure 4).

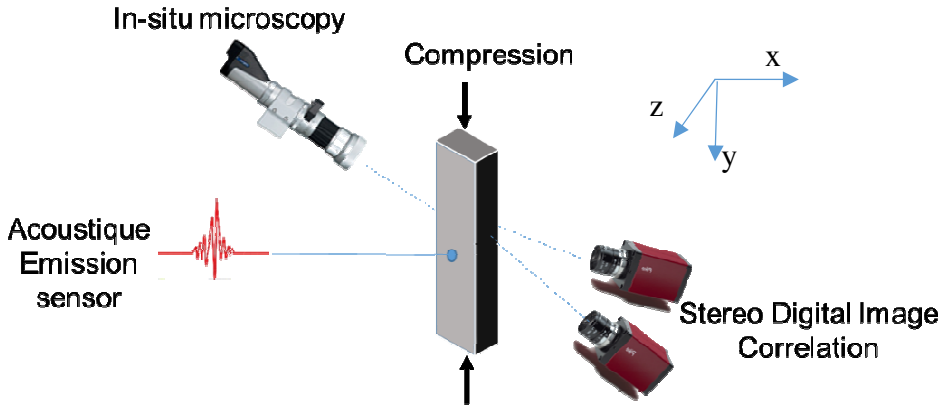

Figure 3 : Representation of all the instrumentation tools and their position in regards to the specimen

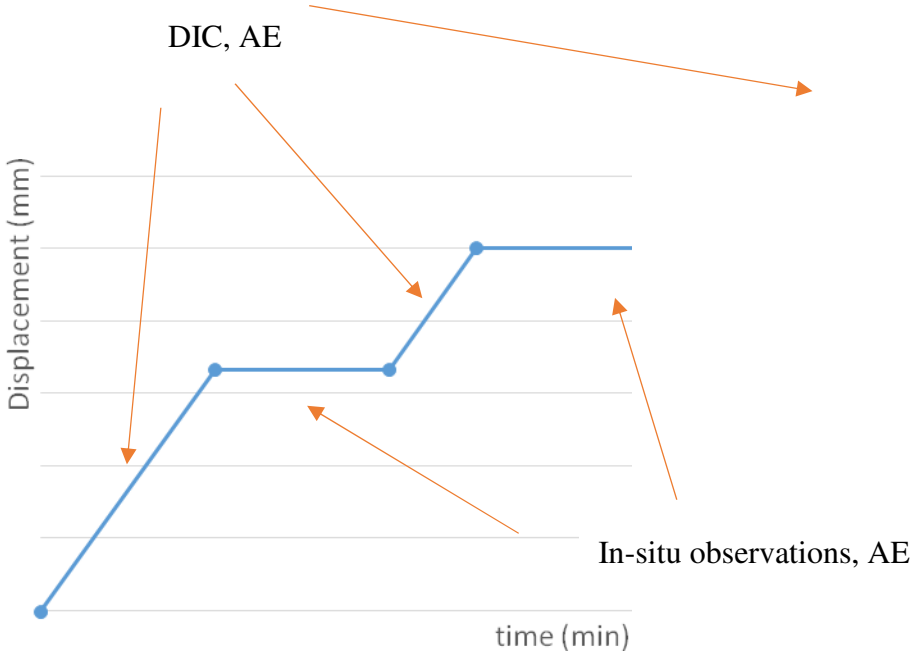

Figure 4 : Schematic representation of the compression testing protocol

Testing was interrupted voluntarily to record observations related to the material under stress (microscopy in-situ). DIC permits to measure strain field on the surface of samples. Stereo-correlation (2 cameras) was preferred in our case to ensure accuracy of measurement and to avoid missing information in the case of mono-correlation (1 camera) related to out of plane displacement. Before starting the measurement, thin dots of speckle were performed on the

surface (the edge of all specimen), with respect of dot size equal to three pixels at least. Relevance and good quality of speckle was systematically controlled before starting the test. Microscopies of the woven architecture were taken before applying the speckle in order to make links with the strain singularities post correlation. Cameras system was pointing to the edge of the specimen giving access to in-plane strain in the loading direction (ε_{yy}) and out-of-plane strain (ε_{zz}). Such parameters should be useful for interfacial damage comprehension [18]. Allied Vision Technologies cameras (2048pixels by 2048pixels) were used with Xenoplan lenses (2.0/28mm-0901) from Schneider Optics. Calibration between the two cameras system was performed for a distance of 40mm from the edge of the specimen with a relative angle of 25°. At the measurement end, correlation was performed on the entire speckle surface using VIC3D software. The strain values were then extracted using virtual strain gauge of about respectively 3mm by 14mm. Figure 3 gives an example of such a virtual strain gauge for the DIC measure. Finally, it is important to point that in this second part of this work, DIC was the only technique of measurement of the strain. Obviously, results given by DIC and strain gauge are in good correlation. In order to be concise, this type of result are well known and mastered, the comparison will not be presented.

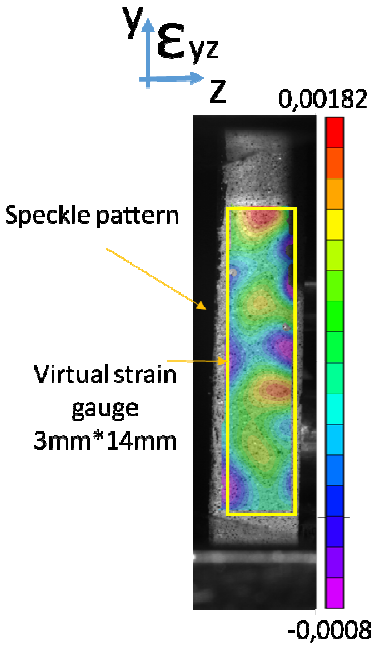

Figure 5 : Example of strain field with the virtual used strain gage

Acoustic emission(AE) setup was used as the major tool for material damage monitoring. It consisted of a sensor (MISTRAS PICO sensors) in contact with the specimen surface. The AE recording (timing parameters in Table 2) threshold and gain were 40dB both (MISTRAS

amplifier). Data processing was performed using AEWIN® software. In these tests, we use only one sensor taking into account the size (compressive free distance 12 mm according to ASTM D-6641).

AE Channel	PDT (µs)	HDT (µs)	HLT (µs)	Max duration (µs)
1	30	150	300	1000

Table 2 : Acoustic emission timing parameters for both used channel[19]. *(HDT: hit definition time; HLT: hit lockout time; PDT: peak definition time)*

The last component of the multi-instrumentation was the in-situ microscopy. For this, HIROX video-microscope was used. Observations were performed on the second edge of the specimen (opposite to DIC). Specimen were polished on the edges before starting the measurement.

Results and discussion

- **Preliminary tests**

Compressive properties in terms of maximum stress and modulus are represented in Table 3. R8 composites show highercompressive strength than the R7. For the compression's modulus, the resin does not have a significant effect. These results demonstrate the influence of the type of resinon the compressive strength. This ascertainment will be discussed in-depth using the multiinstrumentation tools.

Composites	**Strength (Mpa)**	*Standard deviation (%)*	**Modulus (Gpa)**	*Standard deviation (%)*
R7	451,906	4,983	58,350	4,498
R8	503,154	4,096	58,321	3,762

Table 3 : Compressive properties of the materials R7 and R8

- **Multi-instrumented tests**

The damage mode was determined based on the observation for both R7 and R8 materials. The identified damage mode helped to design a supervised classifier for the acoustic emission signals. Then, K-means algorithm was used to acoustic pattern recognition for all the materials. Based on this classification, the last part of the study was an application of the learnt classification method on the R8 material by KNN algorithm (supervised method).

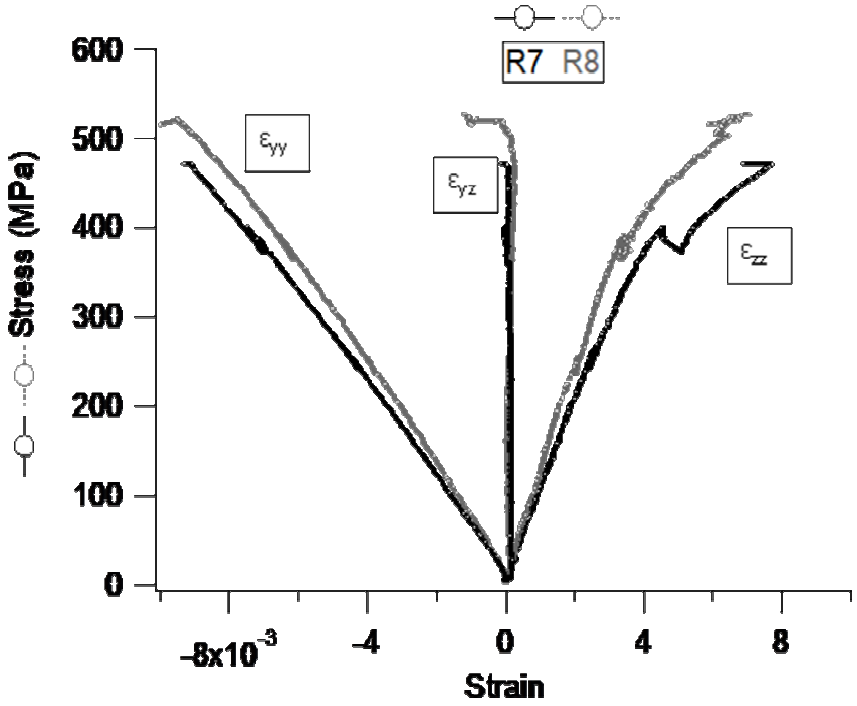

Figure 6 : Stress versus all component of the strain in the (yz) plane forR7 andR8 composites.

As mentioned before the first part deals with the multi-instrumentation results obtained for the R7 composite. In fact, it will be detailed below that damage mechanisms seems to be the same for the R7 and R8 materials. The main difference is in chronological occurrence for each material. This would explain the special interest on the classification of acoustic emission signals (the second part of this section) helping differentiation between the materials with different resin types.

Figure 6 shows the compression stress as a function of the three components of strain obtained by the DIC (ε_{yy}, ε_{zz},ε_{yz}). It is important to recall that the mechanical loading contains holding steps (displacement kept constant) allowing for microscopy observations. This explains the relaxation of the stress noticed on the stress/strain curves. Here, for both materials, we can see that the macro shear strain is insignificant compared to the longitudinal and transversal strain. This finding does not confirm the postulate about contribution of shear mode to the damage mechanism of composites by compression at macroscopic scale. Nevertheless, as we know from literature, the shear stress is typically in concentrated area (tows curvature). In addition, by extracting the strain in relative large virtual strain gauge

(Figure 3), the apparent level of strain might be reduced and even eliminated by the average of positive and negative local shear strains.

Shear strain field maps in Figures 7 are taken at different loading levels. These fields are accompanied by the related microscopy taken before applying the speckle pattern. By this method, direct comparison can be made between DIC strains and the inherent microscopy. The shear strain field map shows strain concentration in some areas of the observed surface (machined edge) of the specimen. Microscopy observation shows that this concentration is localized in the resin area and in ±45 oriented plies. However, at this stage there is no direct proof of its relationship with the fibers curvature even if the design of the weaving architecture seems to influence the pattern of the strain concentrations.

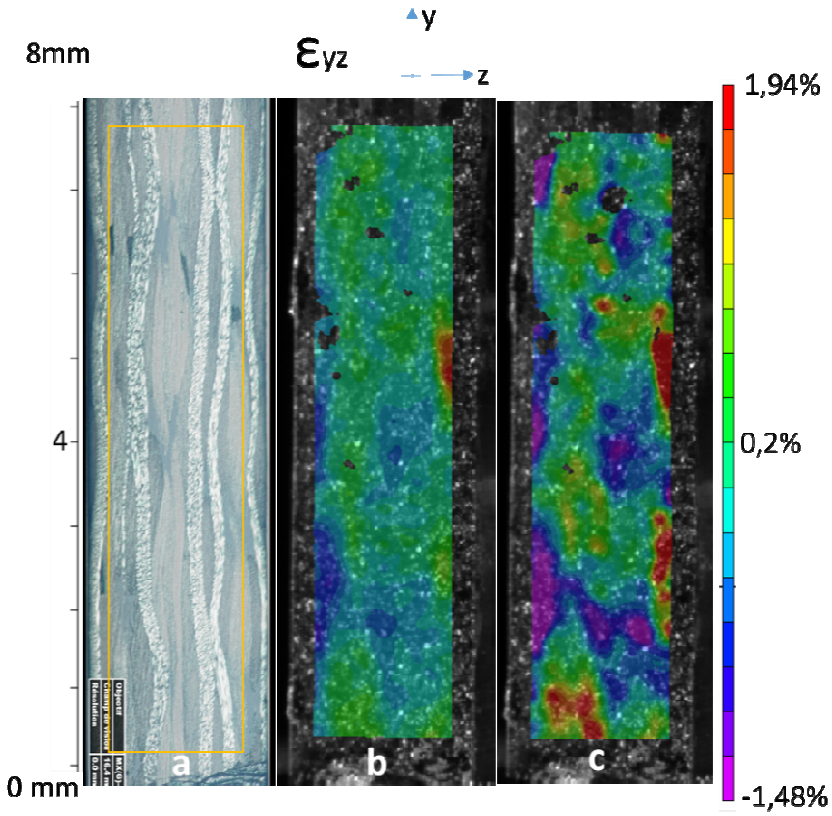

Figure 7 : (a) Microscopy underneath the speckle pattern (before starting the test), and the shear strain field forR7composite with stress level(b) 288MPa (c) 400MPa

The same remarks are held for transverse strain represented in Figure 8. We notice that some areas are subject to local compression leading to local tension of the neighboring zone. This concentration of the strain may be the initiation zone of material failure. With this component of the strain, influence of the ±45oriented plies are more noticeable. Regions of maximum of transversal strain are highlighted in red. The microscopic observation indicates that the high

strain magnitude are localized in the resin pocket area. This area is also highlighted in Figure 7, corresponding to maximum of shear strain.

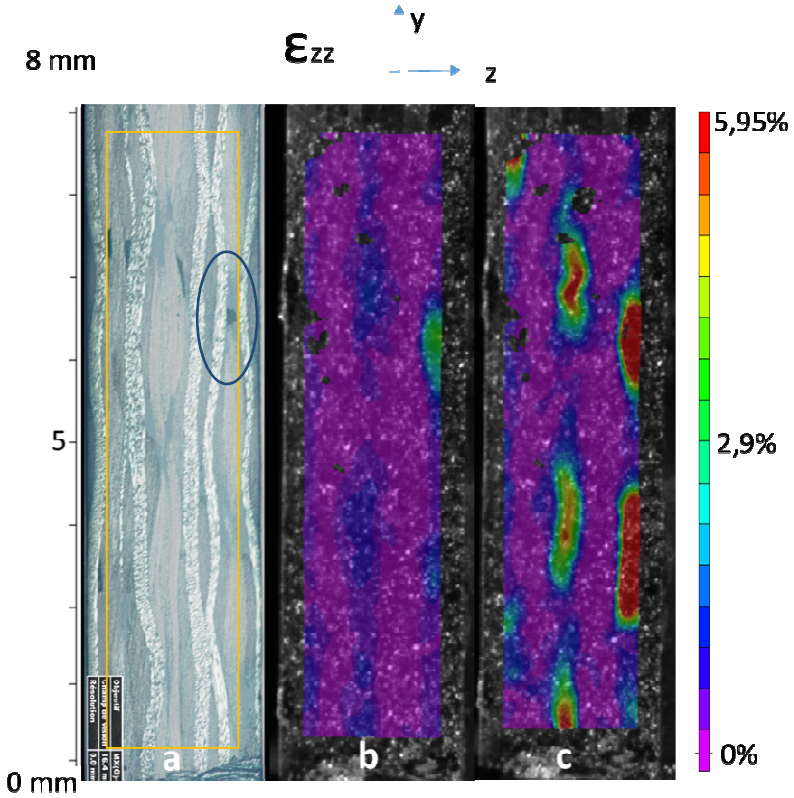

Figure 8 : (a) Microscopy underneath the speckle pattern (before starting the test), transverse strain field for R7composite with stress level (b) 250MPa (c) 400MPa

Figures 9 and 10 represent AE activity during testing in terms of Amplitude (dB) and Acoustic Absolute Cumulative Energy. AE can provide an indication throughout the specimen volume about damage occurring in compression which can be compared with microscopic observations(Figures 11 and 12).

As presented in Figures 11 and 12, by the beginning of the testing, the resin surrounding transversal tows start whitening (color change): which is considered as a sign of plasticity. We also point out the change of color of interfacial zone of longitudinal fibers near the curvature. At this point, AE activity is considerable (Figures 9 and 10), indicating the beginning of the damage by matrix crack and interfacial failure. In fact, acoustic events with amplitude around 70dB are dominant with an absolute acoustic energy slightly increasing.

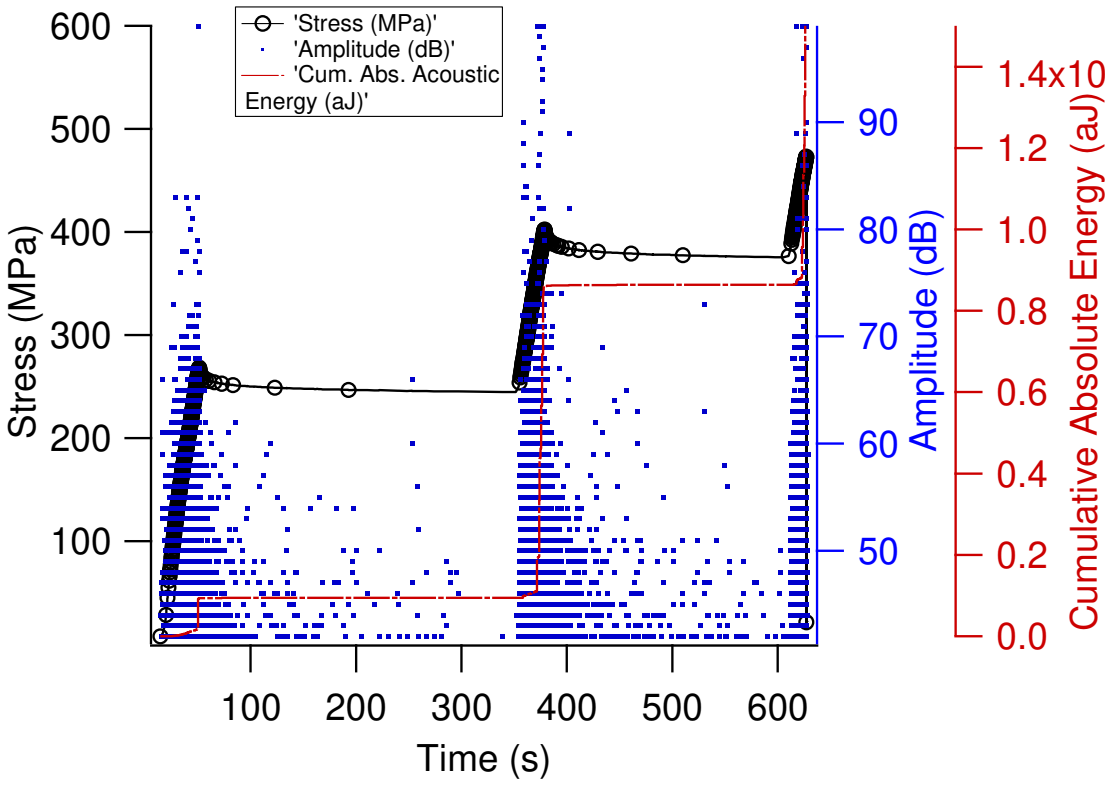

Figure 9 : Acoustic emission activity (Amplitude and Cumulative Absolute Energy) for R7 composite

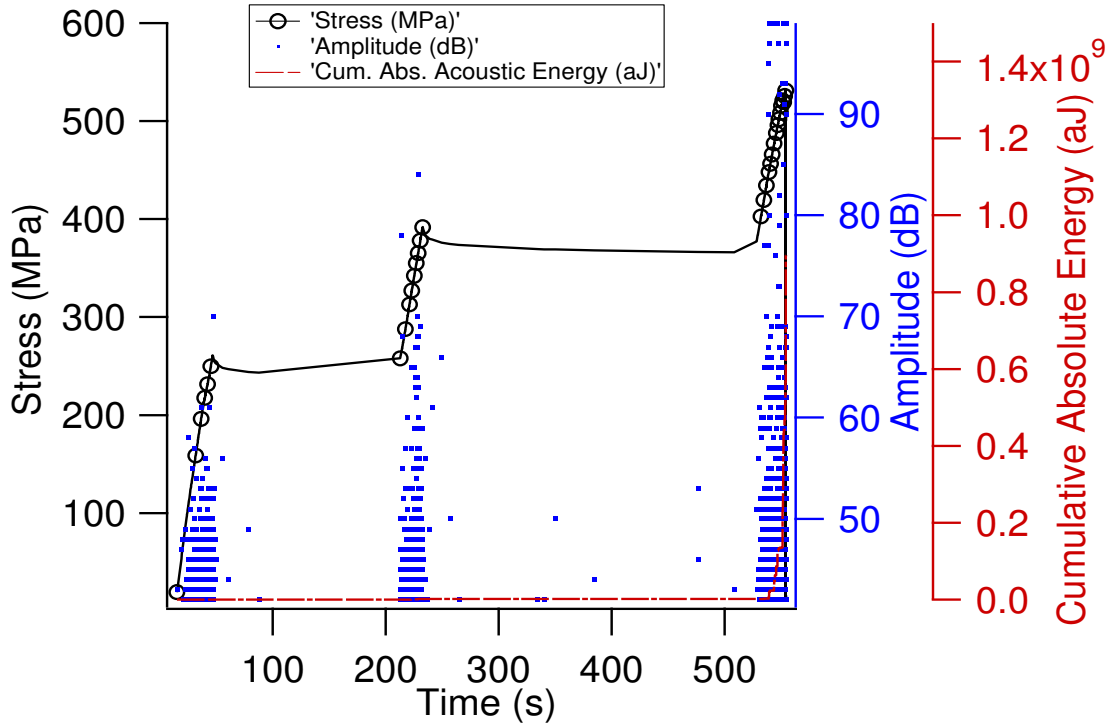

Figure 10 : Acoustic emission activity (Amplitude and Cumulative Absolute Energy) for R8 composite

For the last part of the testing, micro-cracks start to grow (Figures 11(c) and 12 (c)), leading to delamination and longitudinal tows de-cohesion. This second phase is clearly pointed by the AE activity; several acoustic event with amplitude around 90dB and a drastic increase in the absolute acoustic energy (Figures 9 and 10). De-cohesion/delamination of longitudinal fibers is instantly accompanied by fibers fracture and the material final failure (Figures 11(c) and 12(c)).

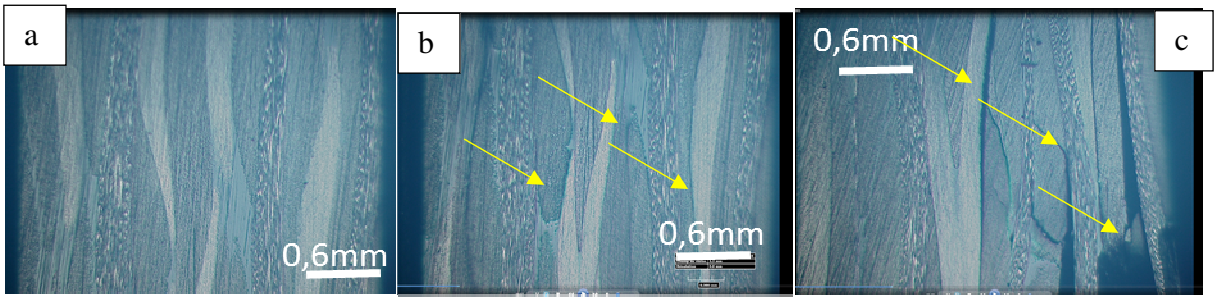

Figure 11 : In-situ microscopic snapshot for R7 composites and for different stress level: (a) 0, (b) 250MPa and (c) 400 MPa

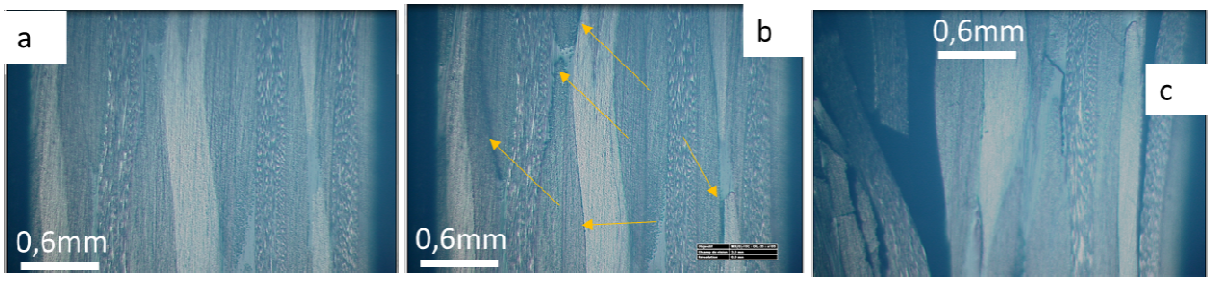

Figure 12 : In-situ microscopic snapshot for R8 composites and for different stress level: (a) 0, (b) 400MPa and (c) 500 MPa

To sum up all the results of our study up to this stage, the same observations are noticed for the R7 and R8 composite except the damage onset. These results indicate that resin effect in terms of compression global properties, does not affect the damage scenario but only its chronological sequence.

To summarize this compression scenario to damage behavior for composites, Figure 13 represents this evolution as cited before with the three presumed stages. Acoustic emission classification is performed and explained in the next section to support these findings.

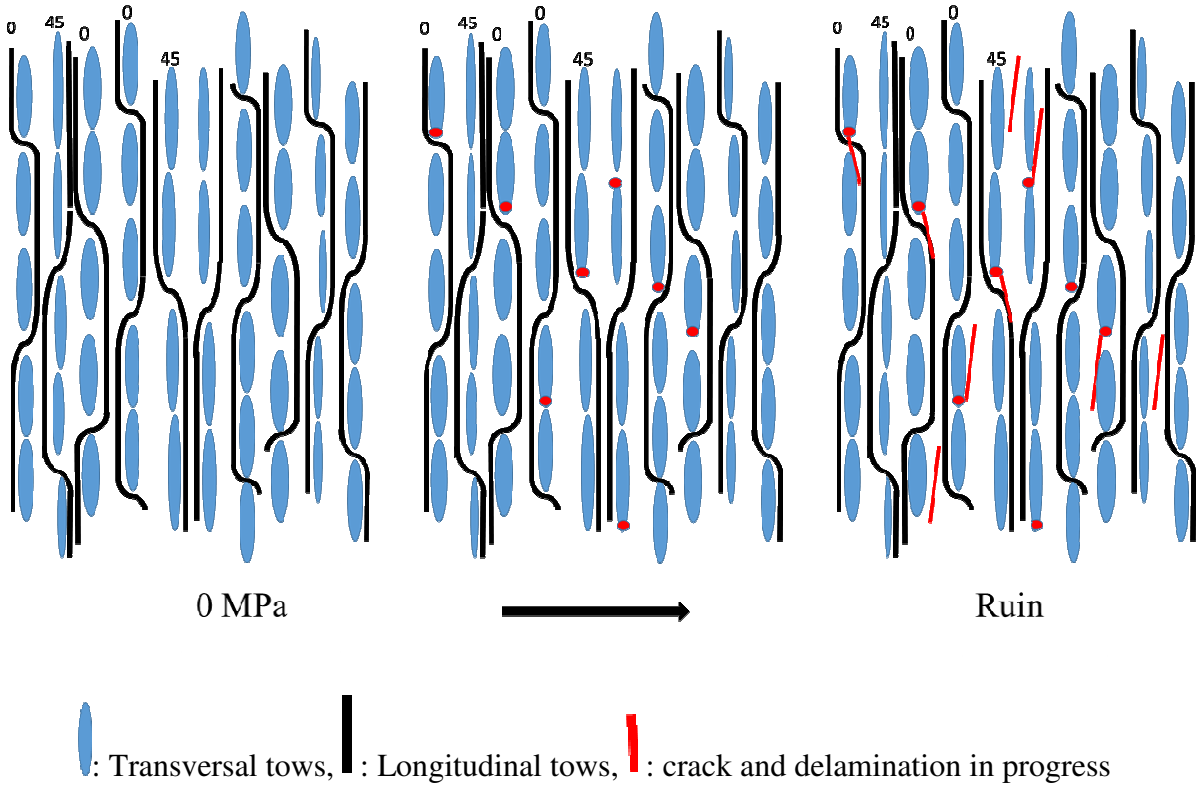

Figure 13 : Damage scenario illustration for all the material of the study

➢ **Classification of acoutic signals: K-means and KNN method**

It is clear that the materials of our study show a weak points heightened by the interfacial zones. The initiation of the micro-damage seems to occur in these areas of the transversal tows. Nevertheless, it clearly does not affect the damage mechanism recorded by the multi-instrumentation tools. It only accelerates the damage occurrence: R8 show higher compression resistance.

❖ Unsupervised method

To go further, the compression properties of composites, acoustic emission signals were processed in order to split the data into families. Each family should be related to a damage mechanism such as matrix crack, delamination or fiber break. At first, unsupervised K-means method was chosen. Preprocessing data consisted on normalizing the data, targeting and keeping the minimum principal descriptors, creating the new basis (formed by the principal component vectors) and creating the projection in the new basis (Figure 14). To perform this analysis, Noesis® software was used.

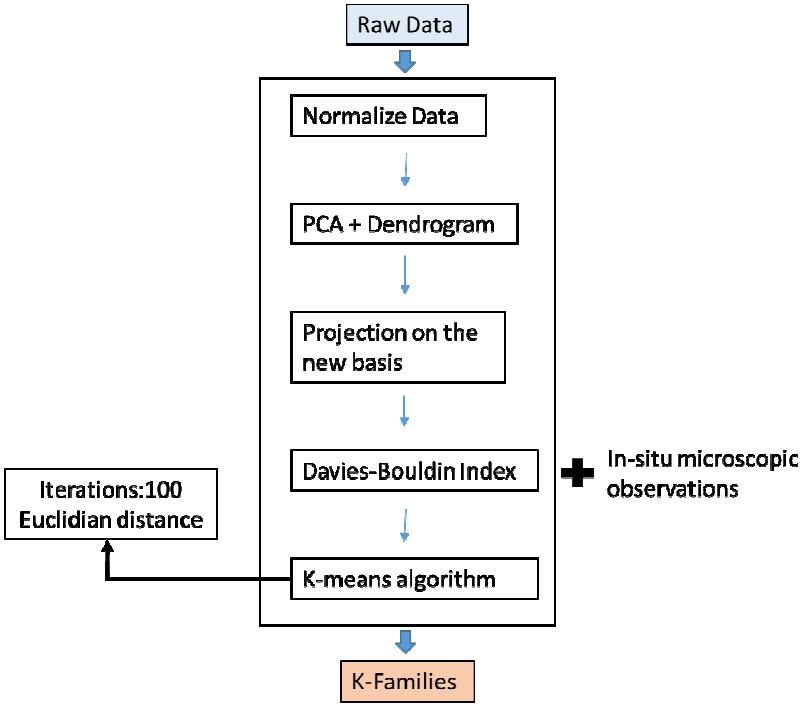

Figure 14 : The Acoustic emission signals classification approach

For the principal vectors' choice, Dendrogram analysis were used. Correlation clearance about 90% was fixed. All vectors showing less than 90% of distance from other components were kept on the final basis. In addition, Principal Component Analysis (PCA) was used to evaluate the correlation between the remaining vectors. At the end of this step, five parameters were judged as completely independent and were kept as the principal vectors of our new basis: risetime, count-to-peak, amplitude, average frequency, absolute energy. It does mean that these five parameters contain more than 90% of the data population signals. These vectors will therefore make it possible to classify the population of clustered signals, which will be linked to the physical phenomena. The definition of every single parameter is explained in the standard related to the acoustic emission technique as non-destructive control tool NF EN 1330-9 [20].

For the K-means algorithm, the number of classes is an important choice. Since it is an unsupervised method, the user oversees of the starting number of families. Nevertheless, some existing criterion could help to find the suitable number of classes for a given population such as the Davies-Bouldin index [21]. The Davies-Bouldin index is a metric for evaluating clustering algorithm. This is an internal evaluation scheme, where the validation of how well the clustering has been done is made using quantities and features inherent to the data set.

To sum up, the idea of this index is to compare the intra-cluster distances, which we want low, with the inter-clusters distance which we want large.

In our case, by applying this index, the number of classes was included between 3 and 4 depending on the sample and the material. By considering the in-situ microscopic observations, it can be hypothesized that the suitable number of classes might be three families:

1- Matrix micro-cracking
2- Delamination and inter-laminar damage
3- Fibers break

Figure 15 and 16 show normalized values radar chart for the R7 and R8 composites for each identified class. We notice that the three classes are quite distinct, which indicate that the classification is relevant. It now remains to attribute to each class a physical phenomena.

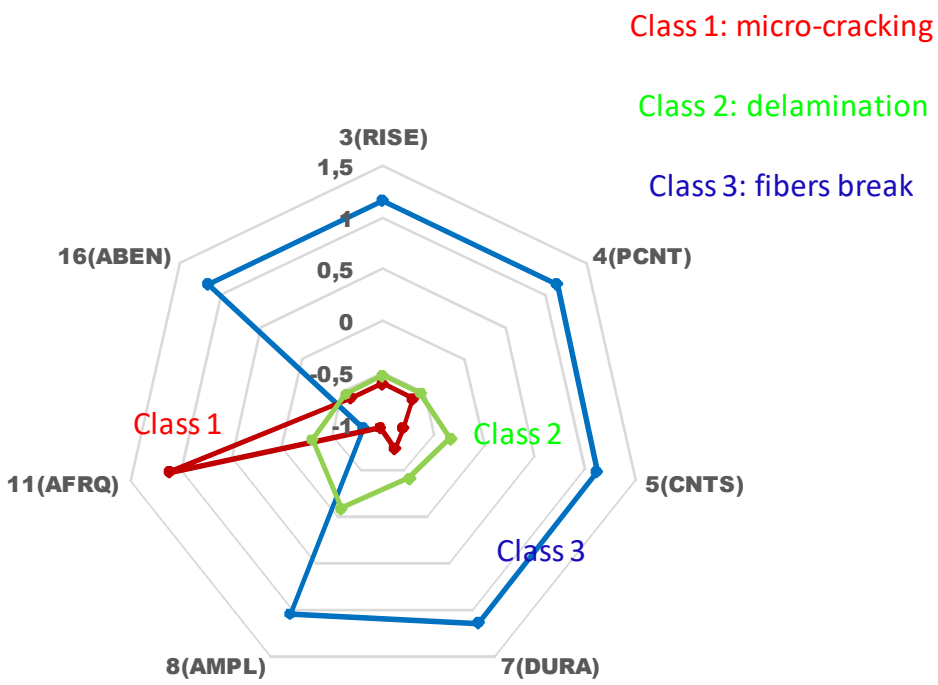

Figure 15 : Normalized values radar chart for the R7 composites for each class and in terms of : CNTS=counts, AMPL=Amplitude, AFRQ=average frequency, PCNT=counts to peak, RISE=Risetime, DURA=Duration, ABEN=Absolute Energy.Class 1 (labeled as noise & matrix micro-cracking), Class 2 (labeled as delamination) and Class 3 (labeled as fibers break)

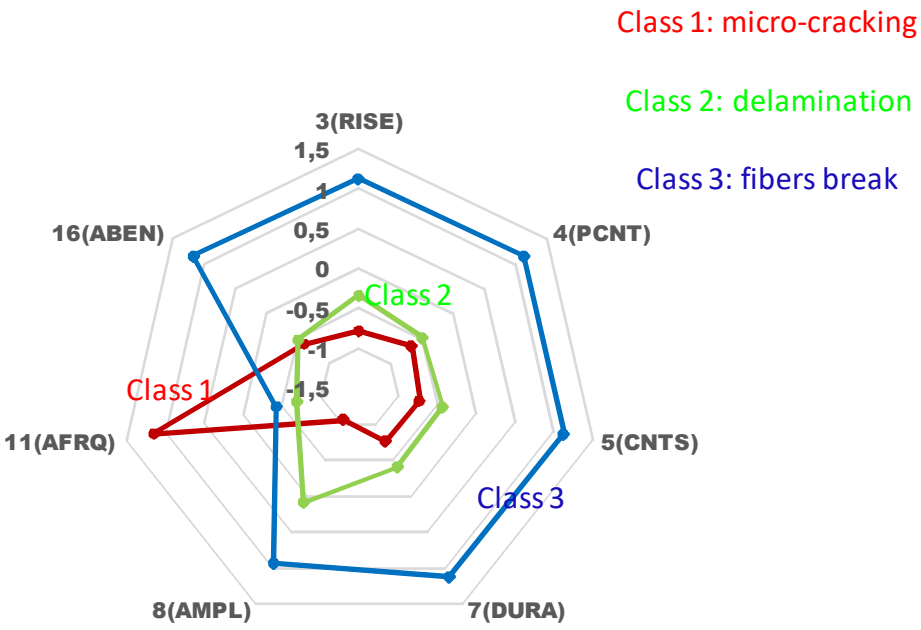

Figure 16 : Normalized values radar chart for the R8 composites for each class and in terms of: CNTS=counts, AMPL=Amplitude, AFRQ=average frequency, PCNT=counts to peak, RISE=Risetime, DURA=Duration, ABEN=Absolute Energy.Class 1 (labeled as noise & matrix micro-cracking), Class 2 (labeled as delamination) and Class 3 (labeled as fibers break)

The friction between the sample/compression-tools or the fibers/fibers, is supposed to cause acoustic 'noise'. In this case, these acoustic events might not have important amplitude or acoustic energy. These signals are potentially considered in the same family by the unsupervised pattern recognition algorithm (K-means in our case). For that, these acoustic signals will be attributed to the first class. At this stage of the study, matrix micro-cracking and acoustic noise are intentionally labeled in the class 1. It remains to attribute classes 2 and 3 to the two other damage mode identified by microscopic observation (delamination/inter-laminar damage and fiber break). For that, we will rely on Figure 15 and 16. These figures show acoustic activity in terms of Absolute Energy during CLC testing. This activity is represented for each acoustic class labeled as mentioned below. It gives first information about class splitting accuracy by analyzing classes overlapping. The second information is about the range of energy for each family: severe events show higher acoustic absolute energy and occur with higher stress level. In fact, *class 1* (micro cracking) starts earlier comparing to class 2 and class 3, for all the materials. The occurrence of class 2 coincides approximately (observation are discrete information and AE is continuous information) for both materials at stress for which we observed the onset of delamination. Microscopic observations (Figure 11 and 12) indicate the delamination onset at 250MPa for R7 and 400MPa for R8 compared to

Figures 17 and 18 giving class 2 onset at 200MPa for R7 materials and 370MPa for R8 materials. We can though attribute the class 2 to the delamination phenomena. The last class to be labeled concern the fiber breakage, it s evident that class 3 carries this information. Indeed, this class, characterized by very high energy and amplitude, arrives at the end of the test and nearly to the failure as shown in Figures 17 and 18.

To sum up, the classification seems to reflect relatively the damage scenario of the materials. The initiation of damage seems to start by delamination and interlaminar damage (class 2). These event are more important as the stress increase. Depending on the used resin, these events seems to start earlier or later At the end of this stage, major damage of the material and the occuring of the final family are no longer far. The fiber breaking (class 3) occurs at the end of the testing. Combination of fiber breaking and delamination is the major cause of the material failure.

Comparing the two materials, the resin effect is mainly on the compression strength and the initiation of micro-damage stress level.

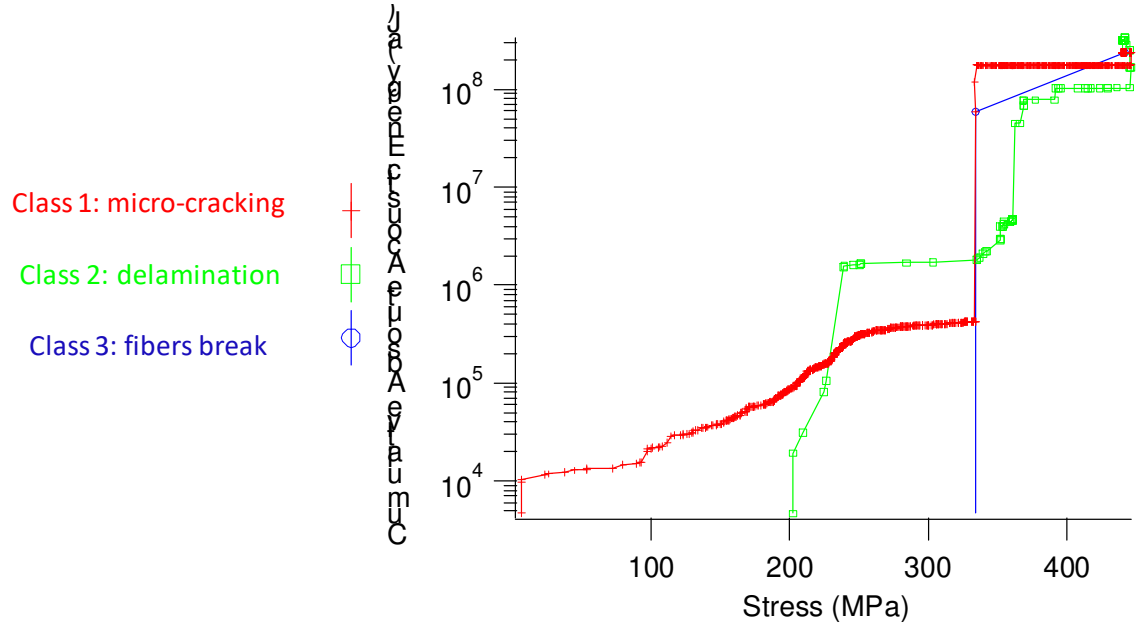

Figure 17 : Cumulative absolute energy vs Stress for each class obtained by k-means method for the R7 composite. Class 1 (labeled as noise & matrix micro-cracking), Class 2 (labeled as delamination) and Class 3 (labeled as fibers break)

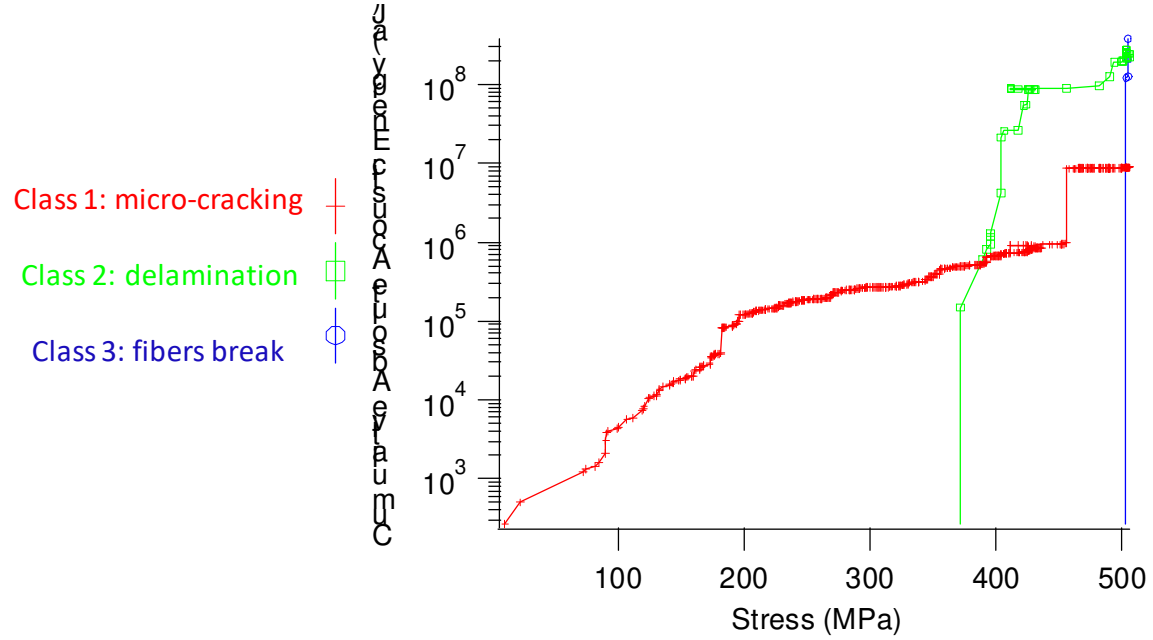

Figure 18 : Cumulative absolute energy vs Stress for each class obtained by k-means method for the R8 composite. Class 1 (labeled as noise & matrix micro-cracking), Class 2 (labeled as delamination) and Class 3 (labeled as fibers break)

Labelling the AE families was frequently studied in the litterature. In our case, based on the centroid of classes (radar charts), a relatively good accordance with several other authors [19, 22–26] considering the difference in terms of mechanical loading. The matrix cracking usually shows AE signals with relatively low amplitude (45-55 dB) and absolute energy. For the delamination, the amplitude (60-70 dB) and the absolute energy are significantly higher but less than the fiber breaking (around 90dB).

- Supervised Method

The evolution of the curves for each class is almost the same for both materials. This means that the damage families labeled by acoustic emission are not dependent on the resin type and the damage mechanisms are the same. The classification performed till this stage of the study was based on the unsupervised method (K-means). It gave us an idea about the different families/classes and the label of each one. Thus, in order to go futher and to verify the K-means classification accuracy, supervised classification was performed.For that, the classification procedure has been enhanced by the KNN method. The R7 composite classes from the K-means method were considered as reference for the KNN method and then was applied to the data of the R8 material. The aim was to control the accuracy of the classes identification (whether classes 0, 1 and 2 are related to acoustic emission occurrence or not). The new classifier was then trained and tested on the known data. Similar method was

performed by other authors for mainly tensile tests of glass fiber reinforced epoxy [19, 27]. Results have shown that this idea is promising but the complete recognition of acoustic pattern is not fully performed. Even if these studies were about different materials, (fibers architecture and types, matrix types) relevance of such approache was proved. Hence, in our study, the multi-instrumental testing method allowed to identify the failure modes and to support the unsupervised patern recognition results. This made the supplementary step of patern recognition algorithm viable and the acoustic signal classes labelization possible.

In our case, error obtained was about 4% which is an accepted score for the supervised method. Then, KNN method was applied to the R8 composite. Figure 19(b) represent the three classes obtained with the new clustering method for the mentioned material. As previous radar representation, seven vectors are drawn in this figure. In Figure 19(a) the R8 radar chart of the Kmeans method is drawn to show the similarity between the results obtained by the two method. Globally, and by analogy with the pervious classification results, the labelization of the obtained classes gives the following order:

- Class 1: labeled as noise & matrix micro-cracking
- Class 2 : delamination
- Class 3 : fiber break

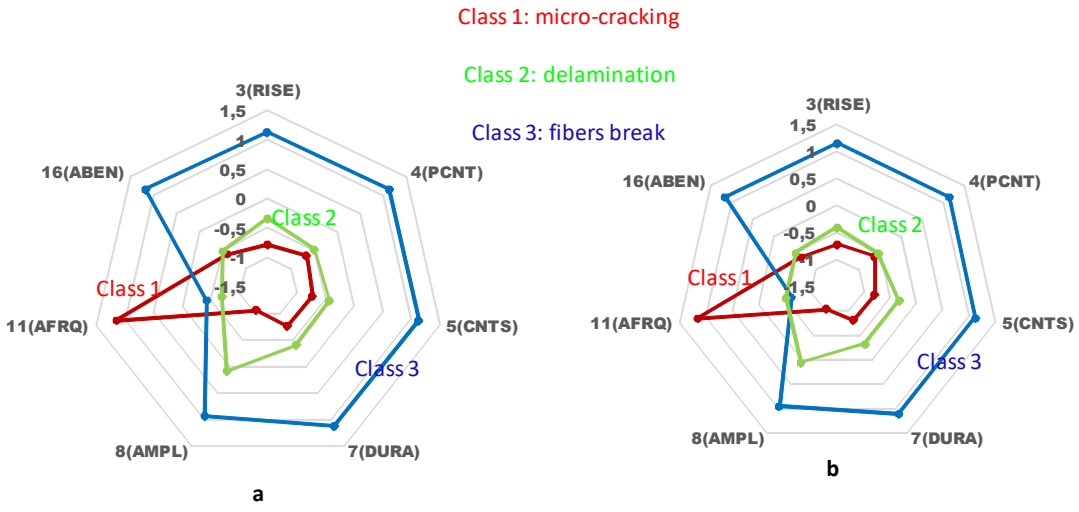

Figure 19 : Normalized values radar chart for the R8 composites for each class and in terms of: CNTS=counts, AMPL=Amplitude, AFRQ=average frequency, PCNT=counts to peak, RISE=Risetime, DURA=Duration, ABEN=Absolute Energy. Class 1 (labeled as noise & matrix micro-cracking), Class 2 (labeled as delamination) and Class 3 (labeled as fibers break), ***(a) K-means method (unsupervised) and (b) KNN method (supervised)***

The use of the KNN method and by taking one material as reference for a different class matrerial confirm that the K-means classification performed in our study was relatively accurate. Also, this unsupervised method could be a starting to elaborate a data base of AE signals to construct a supervied clasifier.

Conclusion:

The aim of our study was to identify the impact of resin on the composite compression behavior. For that, multiinstrumentation technique was deployed in addition to classical compression caracterisation. It appears that the resin modulus affects the compression strength by shifting the maximum stress. By analysing the compression behavior in depth using the DIC, AE and in-situ microscopy, it was found that the failure mechanism scenario is not impacted by the resin properties. The Combination of multiinstrumentation signals allowed to identify damage threshold depending on resin used. This confirmed the influence thetype of resin has on the compression strength. Finally, damage scenario was confirmed by acoustic emission pattern recognition. Three principal families of events were identified and labeled matrix crack, delamination and fiber crack. AE Classification process seems to be promising and the use of supervised classification techniques (ie Knn) seems to improve classes splitting effeciency.

Bibliography

1. Tsampas SA, Greenhalgh ES, Ankersen J, Curtis PT (2015) Compressive failure of hybrid multidirectional fibre-reinforced composites. Compos Part A Appl Sci Manuf 71:40–58

2. Budiansky B, Fleck N-A, Amazigo J-C (1998) On kink-band propagation in fiber composites. J Mech Phys Solids 46:1637–1653

3. Lee SH, Yerramalli CS, Waas AM (2000) Compressive splitting response of glass-fiber reinforced unidirectional composites. Compos Sci Technol 60:2957–2966

4. Odom EM, Adams DF (1990) Failure modes of unidirectional carbon/epoxy composite compression specimens. Composites 21:289–296

5. Kim SJ, Chang SH (2006) The relation between compressive strength of carbon/epoxy fabrics and micro-tow geometry with various bias angles. Compos Struct 75:400–407

6. Opelt C V., Paiva JMF, Cândido GM, Rezende MC (2017) A fractographic study on the effects of hygrothermal conditioning on carbon fiber/epoxy laminates submitted to axial compression. Eng Fail Anal 79:342–350

7. Thompson R (2012) Compressive Strength of Continuous Fiber Unidirectional Composites. Thesis in Clemson University

8. Bai Y, Vallée T, Keller T (2009) Delamination of pultruded glass fiber-reinforced polymer composites subjected to axial compression. Compos Struct 91:66–73

9. Sun W, Vassilopoulos AP, Keller T (2015) Experimental investigation of kink initiation and kink band formation in unidirectional glass fiber-reinforced polymer specimens. Compos Struct 130:9–17

10. Bai Y, Keller T (2011) Delamination and kink-band failure of pultruded GFRP laminates under elevated temperatures and compression. Compos Struct 93:843–849

11. NV C, ST P, P R (2009) Compressive failure of 2D woven composites. In: ICCM Int. Conf. Compos. Mater. p 10

12. Kim J, Shioya M, Kobayashi H, Kaneko J, Kido M (2004) Mechanical properties of woven laminates and felt composites using carbon fibers. Part 1: In-plane properties.

Compos Sci Technol 64:2221–2229

13. Mahadik Y, Hallett SR (2011) Effect of fabric compaction and yarn waviness on 3D woven composite compressive properties. Compos Part A Appl Sci Manuf 42:1592–1600

14. Vieille B, Casado VM, Bouvet C (2014) Influence of matrix toughness and ductility on the compression-after-impact behavior of woven-ply thermoplastic- and thermosetting-composites: A comparative study. Compos Struct 110:207–218

15. Davidson P, Waas AM, Yerramalli CS, Chandraseker K, Faidi W (2012) Effect of Fiber Waviness on the Compressive Strength of Laminated Composites. In: Second Int. Symp. Compos. Mater. Struct. p 1422

16. Jang BP, Huang CT, Hsieh CY, Kowbel W, Jang BZ (1991) Repeated Impact Failure of Continuous Fiber Reinforced Thermoplastic and Thermoset Composites. J Compos Mater 25:1171–1203

17. ASTM D6641 (2015) Compressive Properties of Polymer Matrix Composite Materials Using a Combined Loading Compression (CLC) Test Fixture.

18. Hamdi K, Aboura Z, Harizi W, Khellil K (2018) Improvement of the electrical conductivity of carbon fiber reinforced polymer by incorporation of nanofillers and the resulting thermal and mechanical behavior. J Compos Mater 52:1495–1503

19. Godin N, Huguet S, Gaertner R, Salmon L (2004) Clustering of acoustic emission signals collected during tensile tests on unidirectional glass / polyester composite using supervised and unsupervised classifiers. NDT&E Int 37:253–264

20. NF EN 1330-9 (2017) Non-destructive testing - Terminology - Part 9 : terms used in acoustic emission testing.

21. Davies DL, Bouldin DW (1979) A Cluster Separation Measure. IEEE Trans Pattern Anal Mach Intell PAMI-1:224–227

22. Barré S, Benzeggagh ML (1994) On the use of acoustic emission to investigate damage mechanisms in glass fibre reinforced polypropylene. Compos Sci Technol 3538:369–376

23. Karger-Kocsis J, Harmia T, Czighny T (1995) Comparison of the fracture and failure

behavior of polypropylene composites reinforced by long glass fibers and by glass mats. Compos Sci Technol 54:287–298

24. Harizi W, Chaki S, Bourse G, Ourak M (2014) Mechanical damage assessment of Glass Fiber-Reinforced Polymer composites using passive infrared thermography. Compos Part B Eng 59:74–79

25. Ceysson 0., Salvia M, Vincent L (1996) Damage mechanisms characterisation of carbon fibre / epoxy composite laminates by both eleztrical resistance measurements and acoustic emission analysis. Scr Mater 34:1273–1280

26. Chaki S, Harizi W, Bourse G, Ourak M (2015) Multi-technique approach for non destructive diagnostic of structural composite materials using bulk ultrasonic waves, guided waves, acoustic emission and infrared thermography. Compos Part A Appl Sci Manuf 78:358–361

27. Ech-choudany Y, Assarar M, Scida D, Morain-nicolier F, Bellach B (2017) Unsupervised clustering for building a learning database of acoustic emission signals to identify damage mechanisms in unidirectional laminates. Appl Acoust 123:123–132